Industrial experience on the development of the molten carbonate fuel cell technology

Barbara Bosio [a,*], Paola Costamagna [a], Filippo Parodi [b], Biagio Passalacqua [b]

[a] *Istituto di Ingegneria Chimica e di Processo 'G.B. Bonino' Università di Genova, Via Opera Pia 15, 16145 Genova, Italy*
[b] *Ansaldo Ricerche, Corso Perrone 25, 16161 Genova, Italy*

Abstract

The development of the molten carbonate fuel cell (MCFC) technology at Ansaldo Ricerche (ARI) is reported, starting from small scale single cells up to stacks of several kW capacity. The evolution of material and fabrication strategies as well as the progress in terms of electrical performance are described and discussed. The data reported show that the MCFC technology has been successfully tested on stacks in the kW power class, however some problems still need to be solved to improve the stack performance. In particular, better control of the start-up phase, of electrolyte migration through the manifolds and of the gas feed distribution are required, based on the latest experimental data on a 50 cell stack with cell area 0.1 m^2 (cell active area 0.0702 m^2), which operated for 780 h with a maximum performance of 4 kW at 206 mA/cm^2 at 50% fuel utilisation. Future development steps, which will lead to the realisation and operation of systems of several hundred kW, are presented. © 1998 Elsevier Science S.A. All rights reserved.

Keywords: Molten carbonate fuel cells; Development; Performance

1. Introduction

Fuel cells are today one of the most promising technologies for the production of electrical energy with high efficiency and in environmental respect [1]. Many types of fuel cells (alkaline, polymer, phosphoric acid, solid oxide and molten carbonate ones) are under study at different stages of development. Among them, MCFCs are interesting because of their high operating temperature ($\approx 650°C$), which allows the use of non-noble catalysts. As such catalysts are insensitive to certain fuel contaminants which poison other cells, MCFCs in principle may use a range of gaseous fuels, such as natural gas, biogas or coal gas. Another advantage associated with the high operating temperature is the possibility of cogeneration, which would increase revenue and allow an overall efficiency greater than 80%, with up to 60% electrical efficiency [2].

The technology of MCFCs has received a great attention in the last twenty years, and is now at the stage of scale up to commercialisation. Many developers world wide have shown significant progress [3–5].

In this paper, the experience of ARI in the field of MCFC and stack research is presented. The development strategy of ARI is given in Fig. 1, which also shows present *status* of MCFC technology worldwide.

In an earlier stage of research, stacks with identical cell area and an increasing number of cells were fabricated and operated. Later the cell area was extended to reach commercial size. This program allowed the assessment of the validity of the present technology, defined the operating conditions and established the critical parameters underlying the integration of the stack in the plant.

While basic activities on standard bench-scale single cells are currently being conducted, experimental progress on subscale stacks is now resulting in the development of a ca. 100 kW [6,7] plant. This is a mid-term objective of the Molcare Program [6] leading to the realisation of a MCFC plant that will supply about 250 kW.
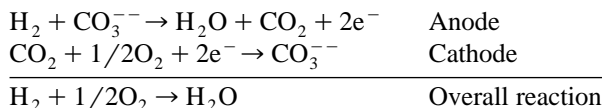
The following sections detail ARI experience on the choice of materials, on cell design and on stack engineering attained during the development process, together with some experimental results obtained.

* Corresponding author. Tel.: +39-10-3532589; fax: +39-10-3532586; e-mail: bosio@istic.unige.it.

2. Single cell development

2.1. Construction technology and experimental apparatus

MCFCs are planar cells formed by a matrix (tile) filled with Li and K carbonates, coupled with two electrodes where the following reactions occur:

$$H_2 + CO_3^{--} \rightarrow H_2O + CO_2 + 2e^- \qquad \text{Anode}$$
$$CO_2 + 1/2O_2 + 2e^- \rightarrow CO_3^{--} \qquad \text{Cathode}$$
$$\overline{H_2 + 1/2O_2 \rightarrow H_2O} \qquad\qquad \text{Overall reaction}$$

The fuel and the oxidant gas are fed separately, and the tile prevents gas crossover and guarantees an adequate ionic conduction and electronic insulation. The single cell is located between two heater plates with the function of temperature control; the contact among the different cell components is maintained by the mechanical load exerted by a hydraulic ram.

Fig. 2 shows the main components that form a single cell.

First ARIMCFCs have been realised in 1981 by hot pressing of the tile (γ-LiAlO$_2$) and cold pressing and sintering of the anode (90% Ni–10% Cr) and the cathode (50% Ni–50% Ag). The anode and the tile were pre-filled with carbonates. Significant results in terms of performance were obtained on a cell tested at atmospheric pressure and at 650°C, which supplied 200 mA/cm^2 at 0.75 V (fuel: H$_2$ 34%, CO$_2$ 22%, N$_2$ 44%; oxidant: air 70%, CO$_2$ 30%). The cell had an active area of 18 cm^2 and was circular; however only square MCFCs were built following this work, since this shape is more suitable for stack design.

The early technology has been improved via a number of steps, as shown in Fig. 3, to achieve the desired performance in terms of endurance, cell size and cost goals.

For example, further developments led to the choice of a ribbed configuration for the anode, obtained by a pressing technique. Such a structure also performed the gas distribution function, so that the normal metallic distributor, which is particularly susceptible to corrosion, was eliminated. In spite of this advantage, this type of anode was difficult to manufacture and very susceptible to creep. For this reason, the present technology is based on tape casting, and the metallic gas distributor is again being used. Current anodes are not ribbed and are similar to those described in the literature [8]. They are fabricated by tape-casting, are composed of Ni–Cr alloyed powders with a chromium content ranging from 2 to 5%, formed by means of heat treatments involving loss of binder, presintering, sintering and chromium selective pre-oxidation [9]. Several studies are in progress to improve their performance and increase their mechanical stability. In this respect Ni–Al anodes are considered promising.

After some tests were carried out using pressed cathodes, the latter are presently prepared by tape casting. A Ni powder slurry is dried, cut into the desired shape, and then sintered. To obtain a lithiated nickel oxide structure a standard process of in situ oxidation is applied during cell start-up [8]. The raw material is presently Ni 255 powder. New cobaltite cathodes are in a test phase as possible alternatives to NiO.

The electrolyte matrix is a tightly packed tile of γ-LiAlO$_2$, with several layers having an overall thickness less than 1 mm. Particular care is required for the selection of γ-LiAlO$_2$ powders to prevent the growth of matrix cracks and the reduction of the cell thickness during operation [8,9]. In the early stages of the development, the electrolyte matrix was placed in the cells in a sintered state; now it is used in the green state. The electrolyte matrix completes its conditioning during start-up, when the binders are removed by combustion or evaporation.
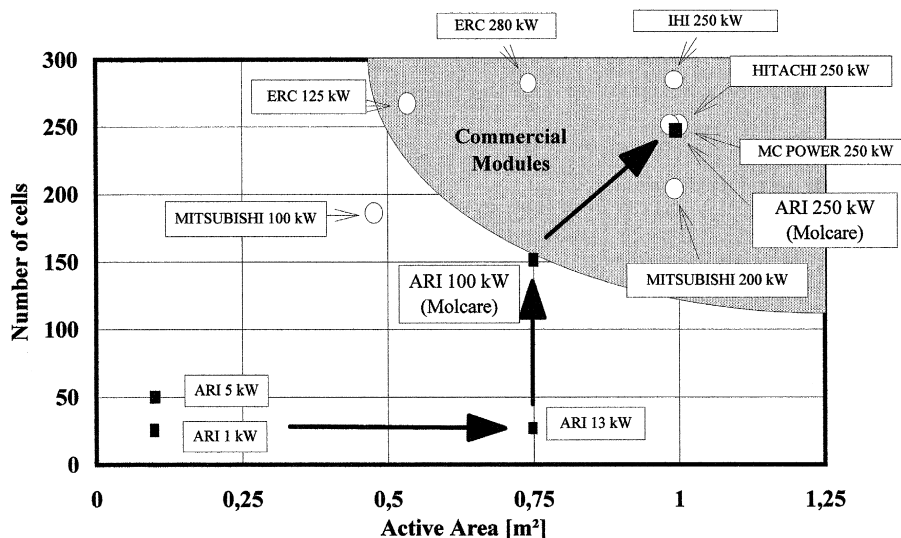

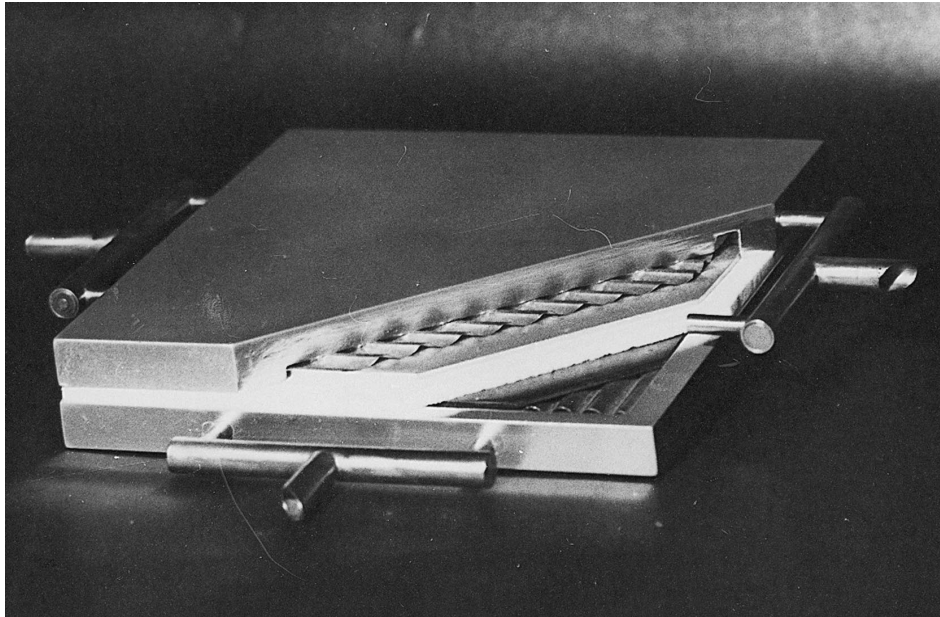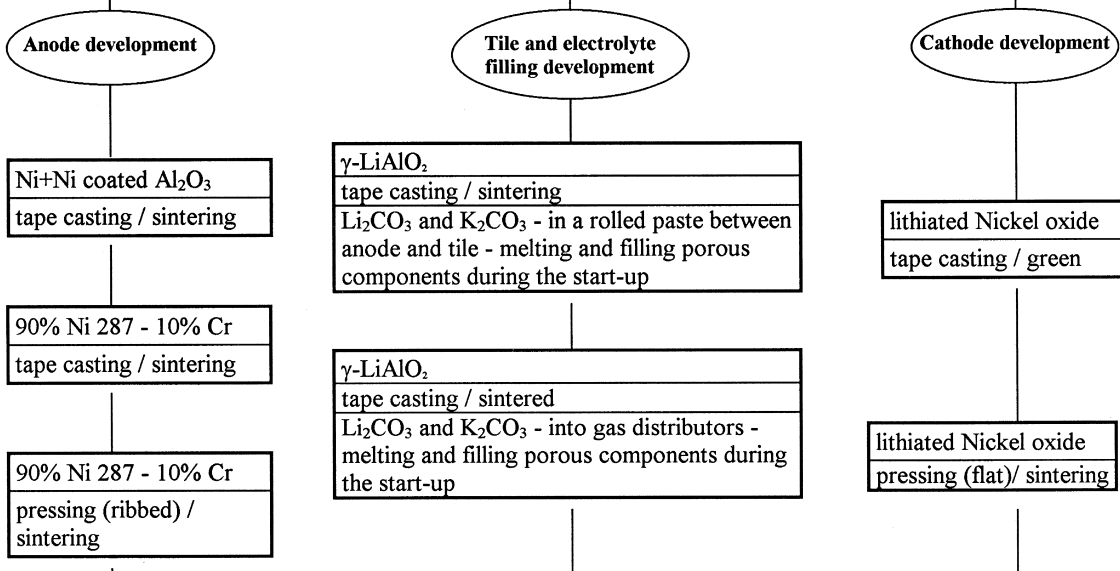Fig. 1. Scale-up of the MCFC stack size up to commercialisation.

Fig. 2. Photograph of a MCFC demonstration cell.

FIRST TECHNOLOGY

	Anode	Tile	Cathode
Materials	90% Ni 287 - 10% Cr	γ-LiAlO$_2$	50% Ni 287 - 50% Ag
Manifacturing	cold pressing / sintering	hot pressing	cold pressing / sintering
Electrolyte filling	Li$_2$CO$_3$ and K$_2$CO$_3$ prefilling in anode and tile		

```
( Anode development )          ( Tile and electrolyte        ( Cathode development )
                                 filling development )
```

Ni+Ni coated Al$_2$O$_3$
tape casting / sintering

γ-LiAlO$_2$
tape casting / sintering
Li$_2$CO$_3$ and K$_2$CO$_3$ - in a rolled paste between anode and tile - melting and filling porous components during the start-up

lithiated Nickel oxide
tape casting / green

90% Ni 287 - 10% Cr
tape casting / sintering

γ-LiAlO$_2$
tape casting / sintered
Li$_2$CO$_3$ and K$_2$CO$_3$ - into gas distributors - melting and filling porous components during the start-up

90% Ni 287 - 10% Cr
pressing (ribbed) / sintering

lithiated Nickel oxide
pressing (flat)/ sintering

PRESENT TECHNOLOGY

	Anode	Tile	Cathode
Materials	90% Ni 287 - 2÷5% Cr	γ-LiAlO$_2$	lithiated Nickel oxide
Manufacturing	tape casting / sintering	tape casting / green	tape casting / sintering
Electrolyte filling	anode pre-filling + Li$_2$CO$_3$ and K$_2$CO$_3$ - into gas distributors - melting and filling porous components during the start-up		

Fig. 3. Development of the MCFC component technology.

The electrolyte is normally a mixture of Li and K carbonates. The ratio between Li and K carbonates is chosen in view of application in stacks. In fact, the migration rate of lithium and potassium ions is different and can lead to a non uniform distribution of the Li/K ratio in the different cells along the stack, and consequently to different physical chemical properties (i.e., melting temperature). In order to avoid this problem, the electrolyte composition has been chosen as 72% lithium carbonate and 28% potassium carbonate, as it has been demonstrated that such composition allows an equal mobility of lithium and potassium ions, eliminating segregation effects at the negative end of the stack [10].

Several procedures have been studied to optimise the electrolyte distribution among anode, matrix and cathode, according to the specific cell configuration. In the past, for instance, the use of a rolled paste replenished with Li_2CO_3 and K_2CO_3 and located between the anode and the tile was successfully demonstrated. At present, the standard system is based on an anode pre-filled by a mixture of Li and K carbonates (pre-filling of about 80% of the free pore volume). Additional electrolyte is placed into the anode gas distributor. When the melting point is reached, the carbonates fill the anode, the cathode and the tile, giving a proper distribution which is a function of their porosities and thicknesses.

To permit the flow of gases into the cell, and to make internal electrical contact, gas distributors and current collectors are respectively used. The size of these components is designed to optimise gas flow distribution and minimise internal electrical resistance [9]. While the current collectors and the gas distributors in previous cells were two separate components, in the latest cells a single element, obtained by die forming, performs both functions. AISI 310 S stainless steel is used at the cathode side; a more complex structure based on a trilayer sheet of Ni clad AISI S stainless steel is utilised at the anode to reduce corrosion.

To complete the single cell hardware, two housings hold all cell components, as shown in Fig. 2. The current housings are aluminised at the borders to reduce metallic corrosion.

After assembling, the start-up process completes the phase of preparation and determines correct cell operation. During this phase the cell temperature is gradually increased up to the operating value, following a linear temperature profile as a function of time, interrupted by a number of planar ranges. This temperature profile is obtained by means of an accurate regulation of the temperature of the heater plates. Gas feed conditions are controlled as well: their temperature is equal to the temperature of the heater plates, and the composition is strongly diluted with respect to the standard values. At the beginning of the process, gases are fed only to the cathode compartment, as the anode channels are replenished with solid electrolyte. After the carbonate melting, the anode compartment is also flushed. As already mentioned, several processes occur

during the start-up: firstly the burn-out of the binders of the electrolyte matrix takes place, then the carbonates melt, and finally the most important reaction occurs: lithiation and oxidation of the cathode (oxidation reaction: $Ni + 1/2O_2 \rightarrow NiO$, Nickel oxide lithiation: $(x/2)Li_2O + (1 - x)NiO + (x/4)O_2 \rightarrow Li_x^+Ni_{1-x}^{2+}Ni_x^{3+}O$) [11,12]. These three processes, which are particularly critical for a satisfactory cell conditioning, occur during the planar ranges of the temperature profile.

2.2. Results and discussion

Results on the operation of a single MCFC are reported below to give an example of the typical performance of present cells. Experimental data are shown for a cell with an active area of 54 cm^2. The anode was a Ni–Cr alloyed powder with a chromium content of 3% and the cathode used Ni 255 as the starting powder. The cell was operated at atmospheric pressure and the two heater plates had a temperature of 650°C. The feed conditions were: fuel composition: H_2 45%, CO_2 9%, N_2 10.6%, H_2O 34.8% (total flow rate 19.8 Nl/h); oxidant composition: CO_2 31.4%, air 68.6% (total flow rate 30.6 Nl/h).

The cell was tested for about 1650 h of hot time (time after electrolyte melting); a characteristic curve obtained after 1460 h of hot time is reported in Fig. 4, showing a typical single cell performance.

Such a cell was characterised by construction technology and operating parameters (described in Section 2.1) very similar to those of stack MCFC7, whose experimental results will be presented and discussed in Section 3.2. Indeed, this test was carried out to check the component materials, to optimise the porous electrodes and to study the behaviour of a single cell for this stack. The starting electrolyte content was higher than the standard value: the initial 'filling level' (% of pore volume filled by electrolyte) was the same chosen for the bottom cell of the stack MCFC7, which was initially flooded, since it would be strongly depleted by electrolyte migration [13] during operation, as Section 3.1 indicates. An additional aim of this test was to check the cell performance under such
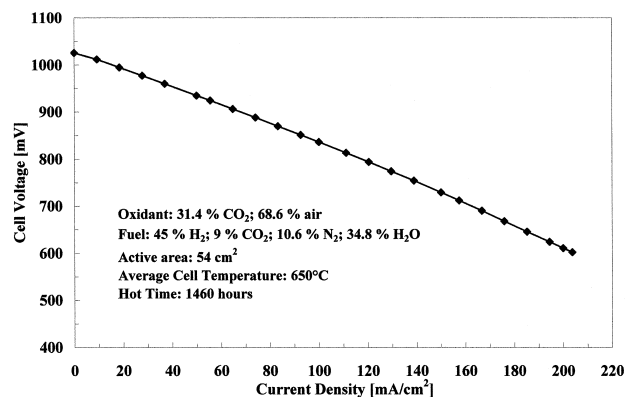

Fig. 4. Performance curve for a single cell.

conditions of flooding and to study the effects of electrolyte losses. In the case of a single cell, electrolyte losses are mainly due to evaporation [2], corrosion, and creep [14].

Fig. 5 shows the behaviour of the cell as a function of time. A considerable improvement in performance is evident, starting from low values early in testing, and reaching the maximum value after about 1460 h of hot time. The early results can be explained in terms of flooding due to electrolyte over-filling. The electrolyte content from 1000 h to 1460 h can be considered in the acceptable range, as the performance of the cell during that period is satisfactory and almost invariable. As a consequence of emptying effects, performance decay is foreseen at some operating time after 1460 h. Data obtained from 1460 h to 1650 h have not been reported in Fig. 5 as they correspond to operating conditions different from each other.

For a further discussion of the effects of electrolyte losses during time, some data collected on a cell similar to the former one but with standard starting electrolyte content are presented in Fig. 6. The feed conditions were: fuel composition: H_2 14.5%, CO_2 11%, N_2 48.5%, H_2O 26% (total flow rate 62 Nl/h); oxidant composition: CO_2 7.6%, N_2 28%, air 64.4% (total flow rate 77.5 Nl/h). The anode reactant concentration being low, the cell performance is lower (OCV ≈ 956 mV) than the one presented in Figs. 4 and 5. This test shows roughly constant results during operating times up to about 700 h.

Two aspects have to be considered in explaining the different behaviour shown in Figs. 5 and 6: (a) the performance of the electrodes is uniform over a wide range of electrolyte filling (at least 10–60%, as reported in the literature [15]); outside this range an abrupt and steep increase of resistance values appears. Analogous results have been found out in the analysis of overall cells [16]. The reason is that at very high electrode filling decay is due to flooding and consequently to reactant diffusion limitations leading to high concentration overvoltages; at low filling levels an higher electrode resistance is ex-
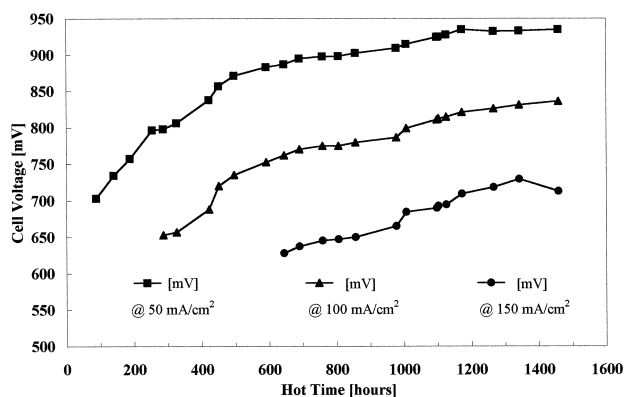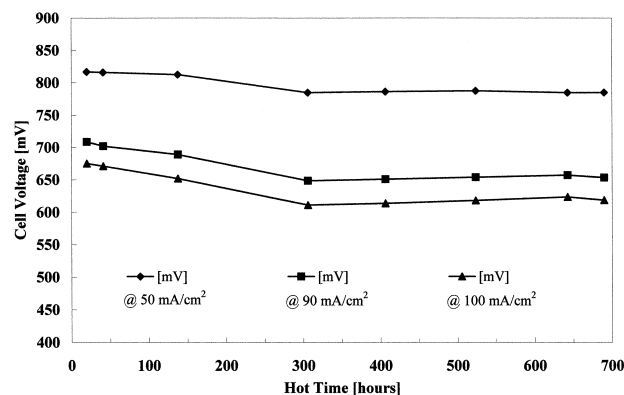

Fig. 6. Behaviour, as a function of time, of a single cell with standard starting electrolyte content (Fuel: H_2 14.5%, CO_2 11%, N_2 48.5%, H_2O 26%, flow rate 62 Nl/h; Oxidant: CO_2 7.6%, N_2 28%, air 64.4%, flow rate 77.5 Nl/h).

pected, for instance due to the difficulties which ions have to move across electrodes [13,14]. The incomplete filling of the electrolyte matrix strongly influence ohmic resistance, gas crossover, gas seal efficiency and corrosion at the cell edges; (b) the electrolyte losses in a single cell, due to corrosion and creepage, have a rate proportional to $t^{1/2}$. Losses due to vaporisation are of some orders of magnitude lower, their trend is linear and their effect becomes important only at high operating times. By summation of the former effects it can be concluded that electrolyte losses proceed quite quickly at low operating times, while the speed is slower and the trend linear afterwards [17].

In the light of the considerations above, it can be stated that: (a) if the starting electrolyte content is within the acceptable range, and the starting electrolyte loss leads to an electrolyte content still in the acceptable range, the cell performance remains stable for a long operating time (such situation corresponds to the cell shown in Fig. 6); (b) if the starting electrolyte content is higher than the acceptable value, losses occurring at low operating times lead the electrolyte content to approach the acceptable range (with a trend proportional to $t^{1/2}$) and the cell performance to improve. This situation is shown in Fig. 5.

Such results demonstrate the importance of a careful electrolyte management to guarantee an acceptable cell performance. The importance of the electrolyte management in stacks will be discussed in Section 3. In stacks this is even more critical, due to the phenomenon of electrolyte migration.

3. Stack development

3.1. Construction technology and experimental apparatus

Details about the operating conditions and the evolution of the construction technology during the scale-up process are reported in Table 1. Eight stacks are described: MCFC1

Fig. 5. Behaviour, as a function of time, of a single cell with high starting electrolyte content (Fuel: 45% H_2, 9% CO_2, 34.8% H_2O, 10.6 1% N_2, flow rate 19.8 Nl/h; Oxidant: 31.4% CO_2, 68.6% air, flow rate 30.6 Nl/h).

Table 1
Evolution of the stack technology during the scale-up process

|		MCFC1	MCFC2	MCFC3	MCFC4	MCFC5	MCFC6	MCFC7	MCFC8	MCFC9
Year		1990	1990	1991	1993	1994	1995	1996	1996/97	Next goal
Cells number		10	10	20	15	50	15	50	20	150
Cell size		0.01m^2	0.1m^2	0.1 m^2	0.1 m^2	0.1 m^2	0.1 m^2	0.1 m^2	0.75 m^2	0.75 m^2
Designed power		170 W	1 kW	2.5 kW @ 4 ata	1 kW	5 kW @ 4 ata	1 kW	5 kW @ 4 ata	13 kW	100 kW
Operating time (hot time)		250 hours	360 hours	300 hours	1604 hours	280 hours	1812 hours	780 hours	1006 hours	---
Operating pressure		1 ata	1 ata	1 ata	1 ata	1 ata	1 ata	1.5 ata	3.5 ata	3.5ata
Separator plates		AISI 310	AISI 310	AISI 310 - wet seal aluminised	AISI 310 - wet seal aluminised	AISI 310 - wet seal aluminised	AISI 310 - wet seal aluminised	AISI 310 - wet seal aluminised	AISI 310 - wet seal aluminised	AISI 310 aluminised
Axial load		Disc springs	Disc springs	Lief springs	Disc springs	Pneumatic bellows	Disc springs	Pneumatic bellows	Pneumatic bellows	Pneumatic bellows
Anode	material	Ni+ Ni coated Al O$_3$ powder	Ni+ Ni coated Al O$_3$ powder	Ni / Cr (10%)	Ni / Cr (10%)	Ni / Cr (10%)	Ni / Cr (10%)	Ni / Cr (3%)	Ni / Cr (3%)	Ni / Cr (3%)
	construction	Tape casting / sintering	Tape casting / sintering	Pressing (ribbed) / sintering	Tape casting / sintering	Tape casting / sintering	Tape casting / sintering	Tape casting / sintering	Tape casting / sintering	Tape casting / sintering
	thickness	0.58 cm	0.58 cm	1.65 mm	0.54 mm	0.54 mm	0.5 mm	0.5 mm	0.5 mm	0.5 mm
	gas distributor	AISI 316	AISI 316	(anode ribbed)	AISI 316	AISI 316	AISI 310 nickel plated	Trilayer sheet Ni/AISI 310/Ni	Trilayer sheet Ni/AISI 310/Ni	Trilayer sheet Ni/AISI 310/Ni
	current collector	AISI 310	AISI 310	(anode ribbed)	AISI 316	AISI 310	AISI 310 nickel plated			
Cathode	material	Li $_x$ Ni $_{1-x}$ O	Li $_x$ Ni $_{1-x}$ O	Li $_x$ Ni $_{1-x}$ O	Li $_x$ Ni $_{1-x}$ O	Li $_x$ Ni $_{1-x}$ O	Li $_x$ Ni $_{1-x}$ O	Li $_x$ Ni $_{1-x}$ O	Li $_x$ Ni $_{1-x}$ O	Li $_x$ Ni $_{1-x}$ O
	construction	Tape casting	Tape casting	Pressing (flat) / sintering	Tape casting / sintering	Tape casting / sintering	Tape casting / sintering	Tape casting / sintering	Tape casting / sintering	Tape casting / sintering
	thickness	0.58 mm	0.58 mm	1 mm	0.54 mm	0.54 mm	0.5 mm	0.5 mm	0.5 mm	0.5 mm
	gas distributor	AISI 316	AISI 316	AISI 316	AISI 316	AISI 316	AISI 310	AISI 310	AISI 310	AISI 310
	current collector	AISI310	AISI310	AISI 316	AISI 316	AISI 310	AISI 310			
Matrix	material	γ Li Al O$_2$	γ Li Al O$_2$	γ Li Al O$_2$	γ Li Al O$_2$	γ Li Al O$_2$	γ Li Al O$_2$	γ Li Al O$_2$	γ Li Al O$_2$	γ Li Al O$_2$
	construction	Tape casting / sintering	Tape casting / sintering	Tape casting / green	Tape casting / green	Tape casting / green	Tape casting / green	Tape casting / green	Tape casting / green	Tape casting / green
	thickness	0.5 mm	0.5 mm	0.46 mm	0.5 mm	0.5 mm	0.5 mm	0.5 mm	0.5 mm	0.5 mm
Fuel source		Bottles	Bottles	Water electrolyser	Water electrolyser	Water electrolyser	Water electrolyser	Water electrolyser	Methanol reformer	Sensible Heat Reformer
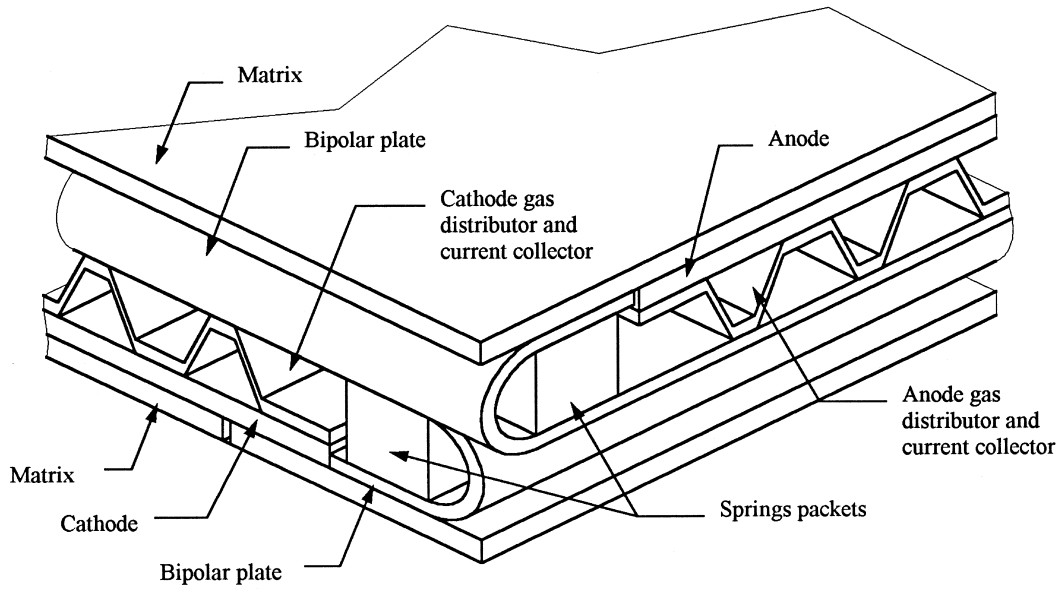
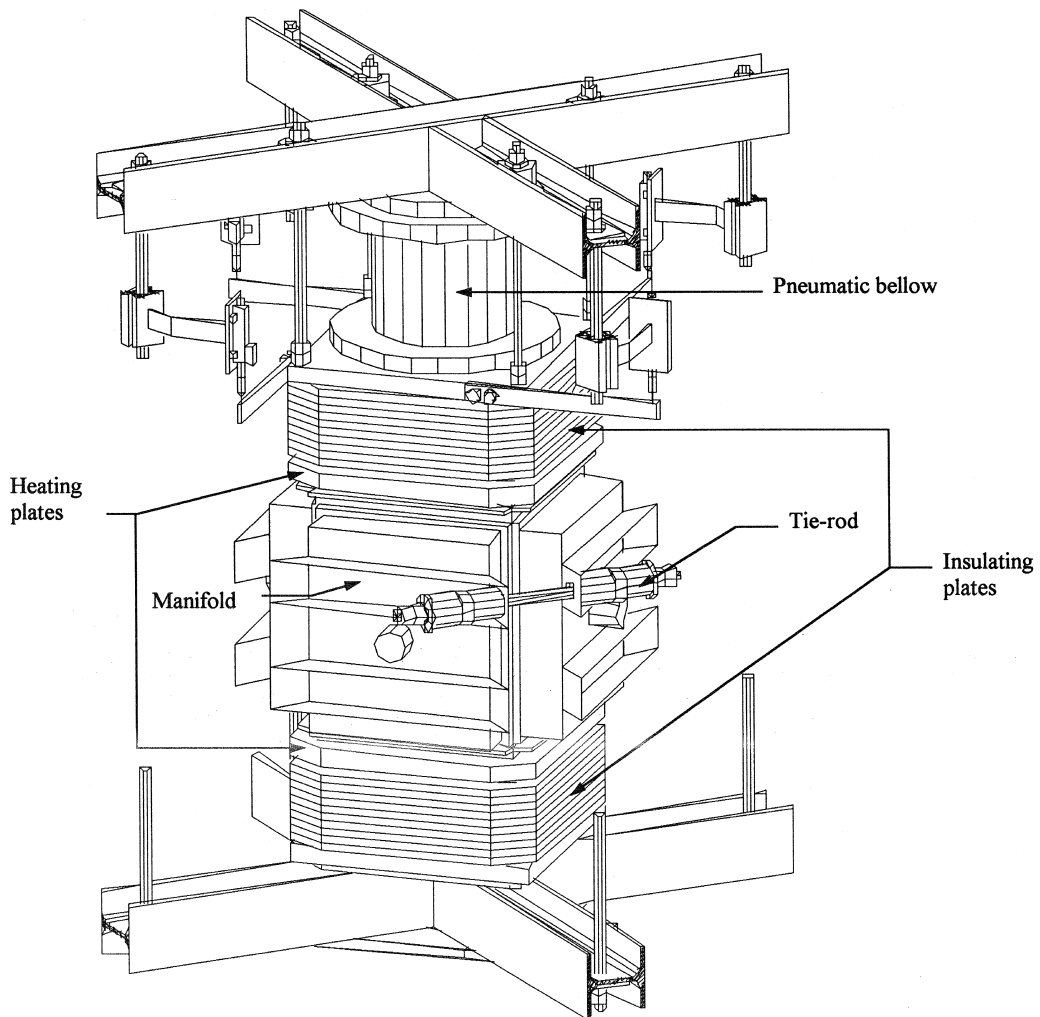Fig. 7. Stack assembly design for MCFC7: detail of the bipolar plates.

Fig. 8. Stack assembly design for MCFC7: main external components.

to MCFC8 were examined during 1990–1997, and showed a progressive increase in the number and size of cells, giving increasing overall power. At the moment stack MCFC9 is under study.

Stacks contain a number of superimposed cells, separated from each other by bipolar plates. The interconnections in the latest stacks (MCFC5 to MCFC8) were as shown in Fig. 7. This solution with folded borders facilitates cross-flow gas feed. Spring packages are inserted in the folds to guarantee a good contact among components and to adjust their mechanical tolerance.

The other main components shown in Fig. 8 are as they appear in the stack MCFC7 assembly drawing.

Two heater plates coupled with insulating layers are placed at the ends of the stack to minimise heat losses. In the single cell the presence of such heater plates guarantees uniformity of temperature. In a stack such a result cannot be achieved, and its only purpose is to regulate the average solid temperature.

The gas feed system works via external manifolds. Previous stacks were assembled with manifolds fixed by bolted bars, for which axial tie-rods later were substituted as shown in Fig. 8. The manifolds are sealed by an assembly of α-alumina, compressed zirconia felt and cloth. During stack operation, the gasket is wetted by the electrolyte and provides a seal that avoids gas leakage across the manifolds. Baffles are introduced in the manifolds to improve the distribution of reactants among the different cells of the stack.

The design of the axial mechanical load has been improved to obtain a good contact among the cell components and a good gas seal on the wet seal area. The previous leaf spring system has been replaced, first by disc springs, and finally by a pneumatic bellows (see Fig. 8). With leaf springs or disc springs the axial load was fixed at the beginning of the test; in this way, a change of pressure in the stainless steel containment vessel resulted in different loads on the stack. In contrast, the bellows system allows a control of bellows pressure as a function of containment vessel pressure to maintain a constant overall axial load during the test.

Electrolyte migration [13] leads to flooding of the top cells and drying of the lower cells during the stack lifetime. To reduce the consequences of migration in the latest stacks (MCFC7 and MCFC8), the starting electrolyte content is higher in the bottom cells and lower in the top ones. Moreover, improved materials on the interface wet-seal/gasket are under study, as well as the possibility of adding bottom and top reservoirs in the form of additional electrodes at the end of the stack. To measure the electrolyte content and composition in each cell of the stack at the end of the stack lifetime, a *post*-test analysis based on a gravimetric test has been adopted [18].

During operation, the stack is fed with an air/CO_2 mixture to the cathodes and with an hydrogen-rich fuel to the anodes. As shown in Table 1, hydrogen is supplied by

different systems for the different stacks. The first stack was fed by cylinders, stacks MCFC3–MCFC7 by water electrolyser and stack MCFC8 by an external methanol reformer.

The start-up process for stacks is carried out by adjusting the temperature profile during time, following the same procedure discussed for single cells.

3.2. Results and discussion

Stacks MCFC7 (50 cells, 0.1 m^2/cell) and MCFC8 (20 cells, 0.75 m^2/cell), fabricated in 1996/1997 are particularly significant in regard to scale-up and for studies on integration of the stack in power plants. In particular, they allowed demonstration of the effects of an increase of cell number or cell area on performance. This experience will be used in stack MCFC9, which will be composed of two modules of 75 cells each with 0.75 m^2 area.

In the following discussion, some experimental results obtained during the operation of stack MCFC7 are reported and discussed. The design parameters and operating conditions are given in Table 1, and a photograph of the stack is shown in Fig. 9. Only preliminary results are available at the moment for stack MCFC8 (nominal power 13 kW). These will be reported in a subsequent paper.

The start-up cycle was carried out by continuously flowing an inert gas mixture (71% N_2, 19% CO_2) in the containment vessel at a pressure slightly higher than that in the manifold ($\Delta P \cong 4$ mbar) in order to avoid leakage from the stack to the vessel. At the end of the start-up
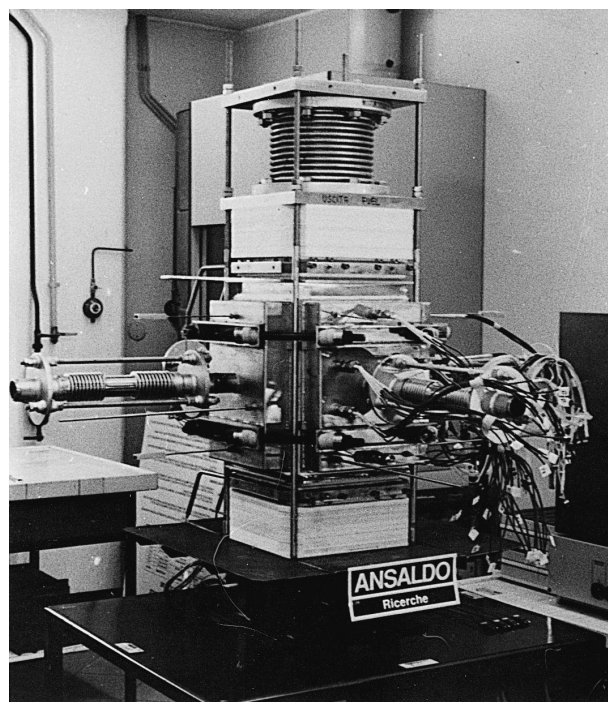

Fig. 9. The stack MCFC7 out of the vessel, without thermal insulation and ready for transfer after operation.
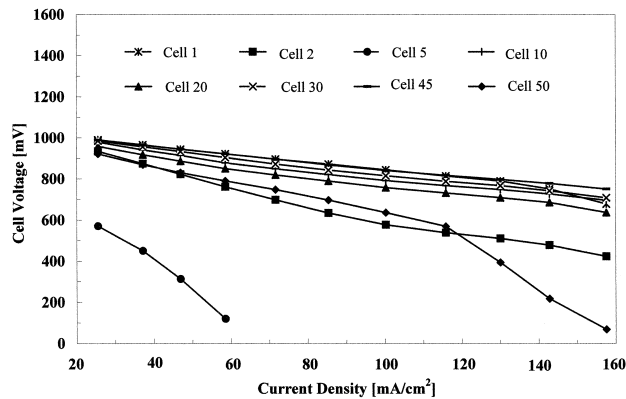
Fig. 10. Performance curves for some single cells of the stack MCFC7 after 528 h of hot time operation at 1.5 ata (Fuel: 25.5% H_2, 8.7% CO_2, 10.7% H_2O, 55.1% N_2, stack flow rate 11,620 Nl/h; Oxidant: 17.4% O_2, 65.6% N_2, 17% CO_2; stack flow rate 50,070 Nl/h). Cells are numbered starting from the bottom. Average solid temperatures are reported in Fig. 12.

cycle an average OCV of 1042 ± 5 mV was measured at approximately 600°C (fuel: 25% H_2, 9% CO_2, 11% H_2O, 55% N_2; stack overall flow rate 11,624 Nl/h; oxidant: 86% air, 14% CO_2; stack overall flow rate 50,130 Nl/h).

The performance curves of some MCFC7 representative cells after 528 h of hot time are shown in Fig. 10 (fuel: 25.5% H_2, 8.7% CO_2, 10.7% H_2O, 55.1% N_2; stack overall flow rate 11,624 Nl/h; oxidant: 17.4% O_2, 65.6% N_2, 17% CO_2; stack overall flow rate 65,000 Nl/h). In addition, the values of the internal resistance of some single cells were measured during the stack lifetime using current interruption. The results are given in Fig. 11.

The stack performance shown in Figs. 10 and 11 is discussed in the following. It can be seen that the performance curves of most of the cells in the stack (for example, Cells 1, 10, 20, 30, 40, cells being numbered from the bottom) are very close to the single cell performance given in Fig. 5. This demonstrates that, in general, cells maintain their characteristics when stacked.

Nevertheless, some of the cells show an anomalous behaviour, which can be due to a number of reasons. For example, random peaks of the value in the internal resistance appear in Fig. 11, which are probably due to structural problems which possibly affected some cells even before assembly. For example, the top cell (Cell 50) showed singular behaviour, with an internal resistance far from typical values. The performance curve of Cell 50 reported in Fig. 10 and shows an increase in slope for current densities larger than 120 mA/cm² (corresponding to a hydrogen utilisation of about 60%), while Cell 2, with an analogous electrochemical behaviour at low current densities, but which was located at the bottom of the stack, does not exhibit such an effect. This phenomenon can be explained in terms of fluid dynamic problems, whose importance has already been underlined for phosphoric acid and solid oxide fuel cell stacks [19,20]. The presence of baffles in the manifolds contributes to a reduction in the problems of non-uniform gas distribution, nevertheless such effects still occur favouring the bottom cells and penalising the top ones in the stack under analysis. Hence, the increase of the slope of the performance curves of top cells is observed when the cell flow rate is not sufficient to supply the overall cell with reactants.

Finally, a group of cells positioned near the bottom of the stack shows a systematic departure from typical cell performance [21], due to the high value of their internal resistance (in particular in Cell 5, which displayed the worst characteristics). This systematic effect could be due to some local problems arising during start-up phase which affected the conditioning of such cells. The importance of an optimised temperature profile during the initial cell lifetime has already been discussed. In the case of single
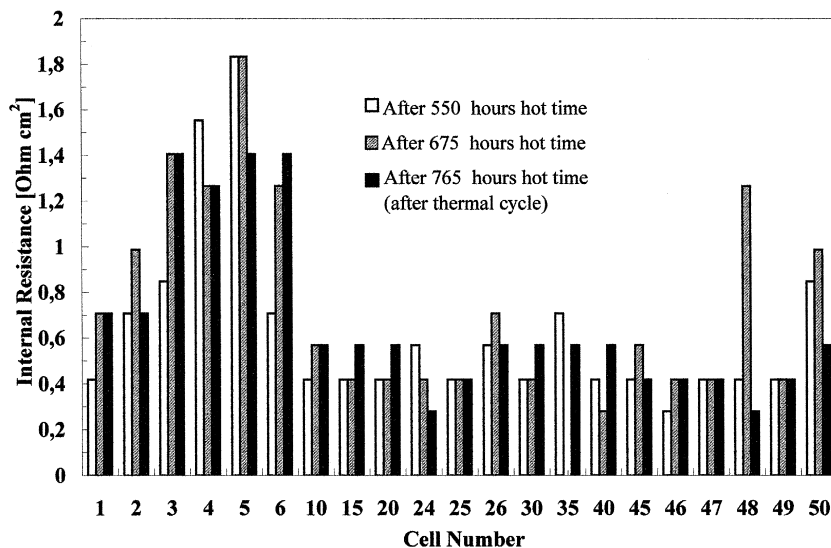

Fig. 11. Internal resistance measured on some sample cells of the stack MCFC7 at different operating times.
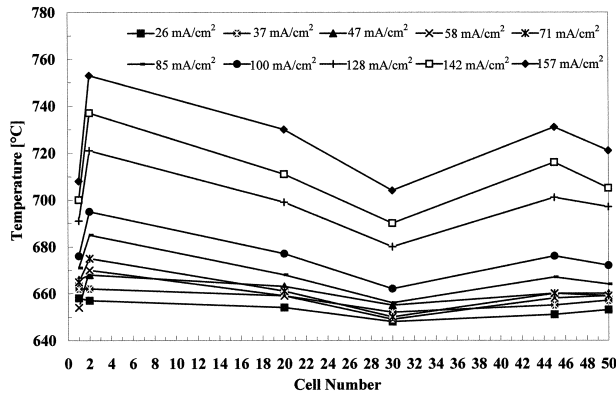
Fig. 12. Temperature distribution along stack MCFC7 at different current densities (Fuel: 25.5% H_2, 8.7% CO_2, 10.7% H_2O, 55.1% N_2, stack flow rate 11,620 Nl/h; Oxidant: 17.4% O_2, 65.6% N_2, 17% CO_2; stack flow rate 50,070 Nl/h).

cells errors of the order of magnitude of a few degrees centigrade may be accurately controlled. However, in stacks, such an accuracy cannot be attained, which explains the problems detected in bottom cells. In addition, we strongly suspect that a defect in the thermal insulation has occurred in this stack which caused lower temperature level in the bottom cells during the start-up phase. In this regard, temperature measurements for Cell 2 detected a difference in the cathode gas temperature of about 48°C between centre and outlet. For the central cells the corresponding temperature difference was about 15°C. The values of internal resistance obtained for Cell 2 are reported in Fig. 11, and show a significant change from typical values. It is worthwhile remarking that Cell 1 displays the lowest value of internal resistance in the bottom cell group, probably because it was exposed to a higher temperature during the start-up, resulting from the presence of the nearby heater plate.

In our opinion, these results demonstrate the importance of the temperature control during the start-up phase, showing that temperature excursions of the order of 50°C from the optimal value can significantly reduce successful start-up. It is important to point out that bad conditioning cannot be remedied during stack operation: in fact, even if the temperature of the bottom cells was satisfactory after the start-up phase (see Fig. 5), the values of the internal resistance did not improve during the stack operating lifetime (Fig. 11). This shows that during the start-up some irreversible basic reactions occur, (i.e., the lithiation and oxidation of the cathode) which are vital to the constitution of the electrode structure.

The thermal response of stack MCFC7 is analysed in the following section.

Fig. 11 shows the effect of a thermal cycle on the internal resistance. This test was carried out to analyse the stack response after solidification and re-melting of carbonates (minimum temperature around 420°C). The slope of the temperature profile vs. time was about 8°C/h during

both the cooling and re-heating processes. The results demonstrate that no significant internal resistance decay occurred after the thermal cycle, ensuring the feasibility of shut-down and re-start cycles.

The distribution of temperature along the stack is shown in Fig. 12 as a function of the overall stack current. The data display an increase in temperature as the current density increases, due to the effect of irreversibilities of the polarisation and ohmic phenomena occurring in the cell. Two *maxima* are visible in the temperature distribution along axial direction, close to the bottom and the top ends of the stack. The high temperature measured near the bottom position results from the high internal resistance, which gives a Joule heating effect. On the other hand, the maximum appearing near top location may be explained by low heat removal due to the low feed gas flow rate. Cells 1 and 50, however, show lower temperatures due to the presence of the end plates, whose temperatures were controlled.

The temperature distribution on the cell plane during operation is shown in Fig. 13 for Cell 30, chosen as an example of standard behaviour. The temperature at the inlet, centre and outlet points along the cathode gas flow direction is given as a function of current density. At current densities between 50 and 70 mA/cm², a decrease of temperature is seen at the inlet position, which is more sensitive to a decrease of temperature of the feed gas. This decrease was imposed to control cell overheating. The temperature at the centre and outlet continuously increases above the inlet temperature as current density increases, due to the increasing effect of polarisation and ohmic irreversibilities.

Several parametric studies have been carried out to test the influence of gas composition and utilisation on cell performance. The effect of the cathode gas composition has been tested by increasing the CO_2 content at the expense of N_2 content (from 14.5% to 33.2% of CO_2) at a constant total flow rate (about 50,000 Nl/h) and under
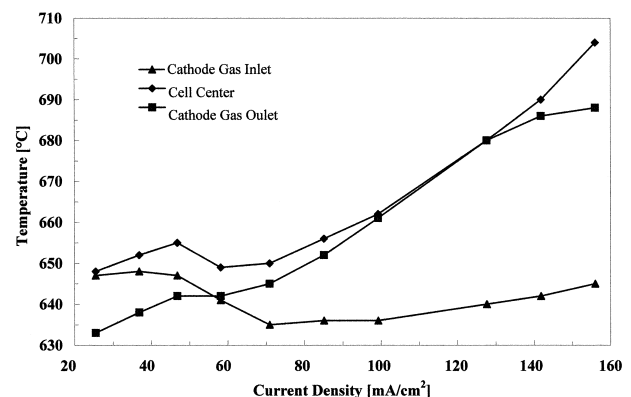

Fig. 13. Temperature of Cell 30 of stack MCFC7 as a function of average current density (Fuel: 25.5% H_2, 8.7% CO_2, 10.7% H_2O, 55.1% N_2, stack flow rate 11,620 Nl/h; Oxidant: 17.4% O_2, 65.6% N_2, 17% CO_2; stack flow rate 50,070 Nl/h).
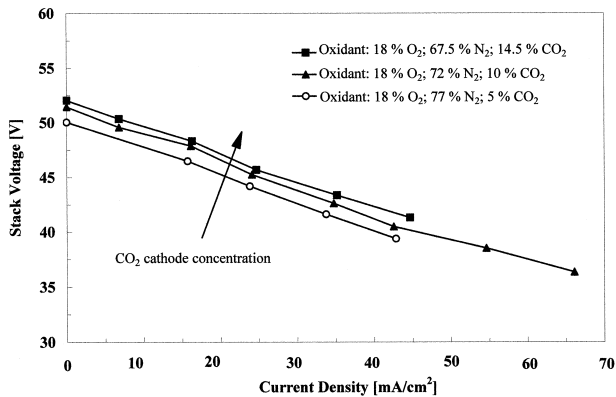
Fig. 14. Effect of variations of the cathode gas composition (Fuel: 25.5% H_2, 8.7% CO_2, 10.7% H_2O, 55.1% N_2, stack flow rate 11,620 Nl/h; Oxidant: stack flow rate 50,130 Nl/h).

Fig. 16. Power supplied by the stack MCFC7 during operation.

constant anode feed conditions. The results of the test is shown in Fig. 14. It demonstrates the expected performance improvement with a CO_2-rich cathode feedstock [15].

Analogous tests have been carried out for the anode gas composition, where the H_2 content has been changed from 12.7% to 25.8% at a total anode flow rate of about 12,000 Nl/h and at a constant cathode flow rate. The results are shown in Fig. 15. As expected, performance increases with the percentage of hydrogen in the feedstock.

Fig. 16 shows the power output of stack MCFC7 during its period of hot time. The stack operated for about 780 h under different conditions, at high current density as well as at OCV. The maximum power was about 4 kW at 206 mA/cm^2 with a fuel utilisation of 50% (fuel: H_2 55%, CO_2 9.3%, N_2 30%, H_2O 5.7%, stack total flow rate 10,864 Nl/h; oxidant: air 83%, CO_2 17%, stack total flow rate 65,430 Nl/h). The main reason why such a performance was lower than the expected nominal power is that the stack was operated at about 1.5 ata rather than the design value of 4 ata, due to some technical problems
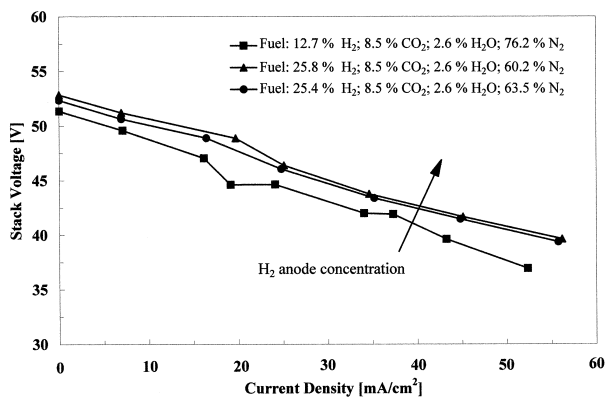
encountered with the pressure controller of the test plant. Nevertheless, such a result can be considered as satisfactory. In fact, at 206 mA/cm^2, the average voltage of the standard working cells was about 0.7 V. The overall performance was penalised, as already discussed, by the anomalous behaviour of certain damaged cells (totally six), which, at 206 mA/cm^2, acted as resistance, causing an overall power dissipation of about 450 W.

Fig. 17 shows the behaviour of some representative cells of the stack MCFC7 as a function of time (fuel: H_2 25.5%, CO_2 8.7%, N_2 55.1%, H_2O 10.7%, stack total flow rate 11,624 Nl/h; oxidant: air 85.6%, CO_2 14.4%, stack total rate 50,130 Nl/h). The performance of Cell 1, flooded at low operating times, shows an increase during lifetime, similar to the cell performance shown in Fig. 5. The speed of electrolyte content variations—and consequently of the performance variations—in the bottom stacked cells is higher than in single cells due to the significant contribution of migration. On the other hand, Cell 30, characterised by a standard starting electrolyte content, shows an almost invariable behaviour, similar to the cell performance shown in Fig. 6. In fact, as already

Fig. 15. Effects of variations of the anode gas composition (Fuel: stack flow rate 11,620 Nl/h; Oxidant: 119% O_2, 71% N_2, 10% CO_2; stack flow rate 50,000 Nl/h).
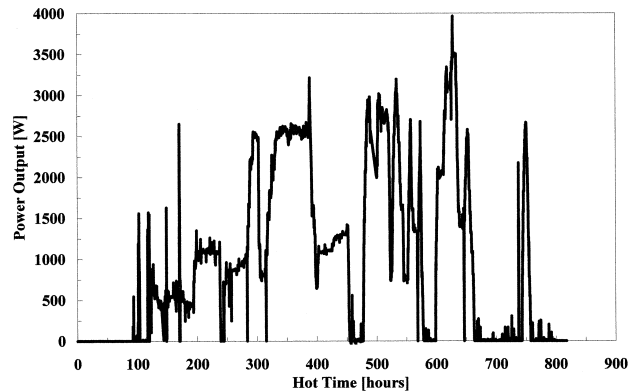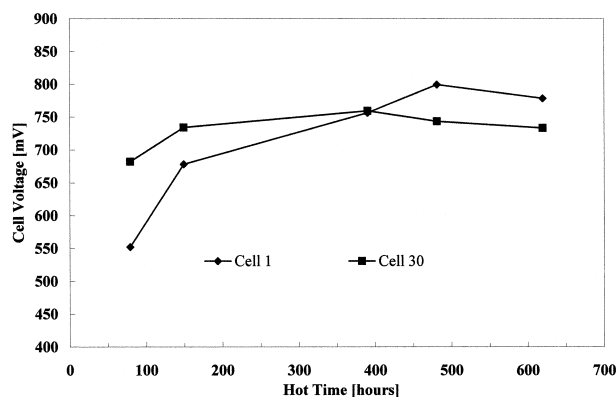

Fig. 17. Behaviour of some representative MCFC7 cells during time (Fuel: H_2 25.5%, CO_2 8,7%, N_2 55.1%, H_2O 10.7%, stack flow rate 11,624 Nl/h; Oxidant: air 85.6%, CO_2 14.4%, stack flow rate 50,130 Nl/h).

mentioned, this stack used differential electrolyte filling along the stack height, with the aim of giving an optimal electrolyte distribution during stack operation, i.e., initial performance was sacrificed to guarantee the desired lifetime.

As discussed, electrolyte losses play a role in stacks, but electrolyte migration is also significant, the stack manifold gaskets being mainly responsible for this phenomenon [22]. Electrolyte migration consists of a progressive movement of CO_3^{--} ions from the top cells (negative pole of the stack) to the bottom ones (positive pole) and of Li^+ and K^+ in the opposite direction. Even if surface tension gradients and electro-osmosis play a role in this phenomenon, the primary cause is the relative ionic movement under an electrochemical potential gradient along the wet-seals and the external manifold gaskets. This process leads to flooding of the top cells, and emptying of the bottom cells during the stack lifetime. Experimental data on earlier stacks indicate that end cells show degradation of performance over time, while central cells show more stable behaviour. In the stack under consideration, the electrolyte content profile changed during the test due to migration effects, leading to a uniform electrolyte distribution at the end of the stack lifetime, which allowed a performance improvement over time. *Post*-test analysis of the various cells of the stack gave similar results for all the cells in regard to the electrolyte content.

The effects of electrolyte losses are partially compensated by the effect of stack compacting. The latter phenomenon consists in a progressive lowering of stack height during operation which involves a consequent reduction of the free pore volume. Hence, the problem of electrolyte losses in the stack is less critical than in the single cell.

4. Conclusions

The development of the MCFC technology at Ansaldo Ricerche has been described, starting from early small scale single cells up to stacks of several kW. Details of the evolution of the fabrication technology have been reported, together with the latest experimental results.

On the basis of the data discussed, it can be concluded that, in general, cells maintain their characteristics when stacked. A further improvement of the stack performance is dependent on the solution of some critical problems. For example, fluid dynamic effects are currently under analysis, since they can limit the feed rate and consequently the power output of certain cells. Another process which requires control to reach optimised behaviour is electrolyte migration along the manifold gaskets from the bottom cells to the top cells of the stack. Finally, the importance of controlling the start-up phase, in particular in regard to the temperature profile over time, has been discussed. We showed that this process is more critical for stacks than for single cells.

The MCFC technology has been successfully proven in small-scale tests, but now needs validation for a complete stack and plant system. This will occur with the design, construction and operation of a 100 kW stack (MCFC9) integrated into a cogeneration plant [6,7]. The scope of the plan is to demonstrate the concept viability of a MCFC on-site cogeneration plant on an intermediate scale and to assess the technical difficulties involved. A 250 kW prototype will be designed, manufactured and operated using the stack MCFC9 test experience as a basis [6].

References

[1] J.H. Hirschenhofer, D.B. Stauffer, R.R. Engleman, Fuel Cells. A Handbook (Rev. 3), DOE/METC-94/1006 (DE94004072), US Department of Fossil Energy, Morgantown Energy Technology Center, Morgantown, WV, 1994.

[2] R.D. Pierce, Proc. Fuel Cell Technol. Status Applications Conf., Chicago, Nov. 1981, p. 67.

[3] Y. Miyake, Y. Akiyama, A. Hamada, Y. Itoh, K. Oda, S. Sumi, K. Nishio, N. Nishizawa, J. Power Sources 61 (1996) 155.

[4] Y. Watanabe, M. Matsumoto, K. Takasu, J. Power Sources 61 (1996) 53.

[5] M. Hosaka, T. Morita, T. Matsuyama, M. Otsubo, Proc. Fuel Cell Seminar, Orlando, Nov. 1996, p. 284.

[6] M. Brossa, A. Dufour, E. Hermana, J.F. Jimenez, F. Sanson, Proc. Fuel Cell Seminar, San Diego, Nov. 1994, p. 238.

[7] F. Parodi, R.A. Sanderson, Proc. Fuel Cell Seminar, San Diego, Nov. 1994, p. 480.

[8] C. Yuh, R. Johnsen, M. Farooque, H. Maru, J. Power Sources 56 (1995) 1.

[9] A. Torazza, A. Dufour, L. Giorgi, J.G. Martìn, G. Rocchini, F.J. Simon, Proc. Fuel Cell Seminar, Orlando, Nov. 1996, p. 371.

[10] H.R. Kunz, L.J. Bregoli, in: J.R. Selman, H.C. Maru, D.A. Shores, I. Uchida (Eds.), Proc. 2nd Int. Symposium on MCFC Technol., Vol. PV 90-16, Electrochem. Soc. Proc. Ser., Pennington, NJ, USA, 1990, p. 157.

[11] E. Antolini, J. Mater. Sci. 27 (1992) 3335.

[12] E. Antolini, J. Mater. Sci. 12 (1993) 1947.

[13] C.D. Iacovangelo, E.C. Jerabek, Proc. Electrochem. Soc. Fall Meeting, New Orleans, LA, Oct. 1984, p. 68.

[14] H.C. Maru, A. Pigeaud, R. Chamberlin, G. Wilemski, in: J.R. Selman, H.C. Maru (Eds.), Electrochemical and Thermal Modelling of Battery, Fuel Cells and Photoenery Conversion Systems, Vol. PV 86-12, Electrochem. Soc. Proc. Ser., Pennington, NJ, 1986, p. 398.

[15] H.R. Kunz, L.A. Murphy, J. Electrochem. Soc. 135 (1988) 1124.

[16] Y. Itoh, Y. Tonoike, Y. Akiyama, M. Nishioka, T. Saito, N. Furukawa, in: J.R. Selman, H.C. Maru, D.A. Shores, I. Uchida (Eds.), Proc. 2nd Int. Symposium on MCFC Technol., Vol. PV 90-16, Electrochem. Soc. Proc. Ser., Pennington, NJ, USA, 1990, p. 169.

[17] J.R. Selman, in: A.J. Appleby (Ed.), Fuel Cells, Trends in Research and Applications, Hemisphere Publishing, WA, 1987, p. 247.

[18] P. Capobianco, M. Leonini, B. Passalacqua, A. Torazza, P. Araldi, M. Scagliotti, G. Strobino, L. Giorgi, S. Scaccia, M. Vittori, A. Colombo, G. Rocchini, in preparation.

[19] E. Arato, P. Costamagna, P. Costa, Chem. Biochem. Eng. Q. 8 (1994) 85.

[20] P. Costamagna, E. Arato, E. Achenbach, U. Reus, J. Power Sources 52 (1994) 243.

[21] A. Torazza, G. Rocchini, M. Scagliotti, Proc. Fuel Cell Seminar, Orlando, Nov. 1996, p. 390.

[22] H.R. Kunz, J. Electrochem. Soc. 134 (1987) 105.